Hindawi
International Journal of Polymer Science
Volume 2018, Article ID 7584281, 13 pages
https://doi.org/10.1155/2018/7584281

Research Article

A Comparison Study of Antiultraviolet and Sustained Release Properties of Polydopamine/Avermectin Microcapsule and Microsphere

Zhichuan Shen,[1,2] **Xinhua Zhou**,[1,2] **Huina Qiu**,[1] **Hua Xu**,[1,3] **Huayao Chen**,[1,3] **and Hongjun Zhou**[1,2]

[1]*School of Chemistry and Chemical Engineering, Zhongkai University of Agriculture and Engineering, Guangzhou 510220, China*
[2]*Key Laboratory of Agricultural Green Fine Chemicals of Guangdong Higher Education Institution, Guangzhou 510220, China*
[3]*Guangzhou Key Lab for Efficient Use of Agricultural Chemicals, Guangzhou 510220, China*

Correspondence should be addressed to Xinhua Zhou; cexinhuazhou@163.com and Hongjun Zhou; hongjunzhou@163.com

Received 28 June 2018; Revised 19 October 2018; Accepted 28 October 2018; Published 30 December 2018

Academic Editor: Ulrich Maschke

By using dopamine (DA) as the monomer, the model drug avermectin (AVM) was loaded on polydopamine microspheres (AVM/PDAMS) and polydopamine microcapsules (AVM@PDAMC) by the method of impregnation and encapsulation, respectively. The materials' structures were systematically characterized using Fourier transform infrared spectroscopy (FTIR), zeta potential analysis, scanning electron microscopy (SEM), thermogravimetric analysis (TGA), and differential scanning calorimetry (DSC). The comparison of antiultraviolet capability as well as release behaviors under different pH values of the materials were studied. The results showed that a spherical appearance was observed from both materials. The use of AVM/PDAMS and AVM@PDAMC made the decomposition temperature of AVM increase to 235°C and 245°C, respectively. After being exposed to ultraviolet light for 1400 min, the residual ratios of AVM of AVM/PDAMS and AVM@PDAMC were 42% and 54%, respectively. Both AVM/PDAMS and AVM@PDAMC showed acid sensitivity. AVM/PDAMS and AVM@PDAMC took about 13 h and 60 h to reach the release rate of 50% under pH 3. The release process of AVM/PDAMS could be explained by the Weibull model at pH 3, while the release behavior of AVM@PDAMC fitted the Baker–Lonsdale equation. At pH 7 and pH 9, both of the delivery materials followed the Korsmeyer–Peppas model and belonged to the Fick diffusion.

1. Introduction

Pesticides are widely used to control insects, plant diseases, and weeds. However, due to climate conditions and the administration model, most of the applied pesticides decompose before reaching their targets [1]. The pesticides deposited onto plants are easily decomposed or volatilized due to exposure to the sun and are leached into the soil with the rain water [2, 3]. To avoid such degradation and waste, the methods of encapsulation or adsorption of the pesticide with a suitable vehicle are used in this field to provide the properties of controlled release as well as responsiveness to the environment [4, 5].

Several delivery systems have been developed for loading pesticides [6, 7]. Among them, polydopamine (PDA) nanoparticles obtained from the autoxidation of its dopamine (DA) have attracted wide attention in the past few years. For PDA microspheres, in a weak alkaline solution (pH = 8.50), DA monomers can be oxidized to a quinoid structure. Then, the intramolecular cyclization and oxidative rearrangement will take place via the 1,4-Michael addition reaction to form 5,6-dihydroxyanthraquinone. Finally, all these structures will self-polymerize to form the PDA microspheres through physical interaction or covalent bonding [8]. For PDA microcapsules, by using an oil droplet as a soft template, it can enrich the hydroxide ions spontaneously at the

oil/water interface and provide it a negative potential so that the in situ emulsion interfacial polymerization can be used to prepare PDA microcapsules [9, 10]. Yu et al. [11] investigated the loading and release behavior of PDA microcapsules on the mitochondrial marker Rh6G and found that the drug release process showed pH responsiveness. Ho and Ding [12] found that the PDA microspheres exhibited pH responsiveness during the controlled release of the anticancer drug camptothecin. Tamanna and Yu [13] loaded the antimicrobial rifampicin on PDA microspheres and found that the system maintained high stability at an acidic pH. This material has garnered important interest in the application of the controllable release of drugs as it can be governed by the responsivity of the molecular chains or the surface charge in reaction to pH [14–17]. Moreover, studies have shown that PDA can absorb ultraviolet light, which is why it is widely used in the preparation of UV-shielding composites [18–24]. Although both systems use only PDA as the carriers, drugs are loaded on the surface of PDA microspheres by means of an adsorption method, while the loading of drugs in PDA microcapsules employ a coating method. The different loading methods inevitably lead to differences in the structure, properties, and drug release behavior. To the best of our knowledge, fewer studies have paid much attention to the difference in UV resistance as well as the controlled release behavior of pesticides between the PDA microspheres and the microcapsules. Hence, the difference between these two systems requires more research.

The biological pesticide avermectin (AVM), a kind of macrocyclic lactone, is commonly used in agriculture by virtue of its insecticide and acaricide activities [25]. On one hand, research has shown that AVM is susceptible to photolysis and oxidation, leading to its instability under exposure to UV light and a short half-life [26]. On the other hand, the structural composition of AVM contains a large number of hydroxyl and aromatic heterocycles, which can be adsorbed onto the surface of PDA or encapsulated by a PDA coating by the formation of π–π stacking and hydrogen bonds [27]. This connection allows the PDA delivery systems to exhibit properties of pH responsiveness and controlled release. Therefore, AVM can be applied as a model drug for studying the difference of release behaviors between the PDA microspheres and the PDA microcapsules as well as their UV resistance.

Herein, AVM was loaded on the PDA microspheres and microcapsules by the method of wet-impregnating adsorption and encapsulation, respectively. The differences in structure, antiultraviolet performance, and release behavior of the two systems were analyzed with a series of characterization tests. The release mechanism was also revealed to provide a useful reference for the field of controlled release of pesticides.

2. Materials and Methods

2.1. Chemicals. 3-Hydroxytyramine hydrochloride (DA) and 1,1,1-tris(hydroxymethyl)-methanamin (Tris) were all obtained from Shanghai Aladdin Biochemical Technology Co. Ltd. (Shanghai, China). Ethanol, 1-butanol, sodium hydroxide, and hydrochloric acid were obtained from Tianjin Damao Chemical Reagent Factory (Tianjin, China). Avermectin (AVM, wt = 97%) was obtained from Henan Kai Rui Biotechnology Development Co. Ltd. All chemicals were of analytical grade and used as received without any further purification.

2.2. Synthesis

2.2.1. Preparation of Polydopamine Microsphere and Its Adsorption for Avermectin. According to the literature [28, 29], 200 mL (0.02 mol/L) of Tris solution (pH = 8.50) was added to a flask to be completely stable at 25°C with 30 min of stirring. Then, 200 mg of DA was added to the solution and the reaction was stirred for another 24 h before being filtered, washed, and dried at 70°C. The samples were denoted as PDAMS. After that, 25 mg of PDA was immersed in a 50 mL ethanol solution with 150 mg of AVM at 30°C under stirring for 24 h before being filtered, washed, and dried at 60°C [30]. The samples were denoted as AVM/PDAMS.

2.2.2. Preparation of Polydopamine Microcapsule and Its Encapsulation for Avermectin. According to the literature [10], 200 mL (0.02 mol/L) of Tris solution (pH = 8.50) and 20 mL of 1-butanol solution with 200 mg AVM were added to a flask to be completely stable at 25°C with 30 min of stirring. Then, 200 mg of DA was added to the solution and the reaction was stirred for another 24 h before being filtered, washed, and dried at 60°C. The samples were denoted as AVM@PDAMC. The preparation of polydopamine microcapsules without AVM was synthesized in the same method and denoted as PDAMC. The above synthesis processes are shown in Scheme 1.

2.3. Testing the Adsorption and Encapsulation Properties. A UV Lambda 365 ultraviolet-visible spectrometer from PerkinElmer (Waltham, MA, USA) was applied to measure the amount of AVM loaded on the PDAMS and PDAMC. A linear regression for the relationship between the solution concentration (C) and absorbance (A) of the AVM standard solutions at different concentrations was performed at $\lambda = 245$ nm to obtain a standard curvilinear equation: $A = 0.028C - 0.0655$; $R^2 = 0.9997$. UV spectroscopy was used to measure the absorbance of this solution before and after the adsorption in AVM ethanol solution.

Loading content (LC) of AVM/PDAMS was calculated by the following equation:

$$\mathrm{LC} = \frac{[(C_0 - C_t) \times V]}{[M_1 + (C_0 - C_t) \times V \times 0.001]}, \quad (1)$$

where C_0 is the original mass concentration (mg/L) of the AVM ethanol solution, C_t is the mass concentration (mg/L) of the AVM ethanol solution at the relevant time interval, V is the volume (L) of the ethanol solution, and M_1 is the mass (g) of the PDAMS.

According to [31], the operational method to calculate the loading content (LC) of AVM@PDAMC is as follows: 50 mg AVM@PDAMC was dispersed in a flask containing

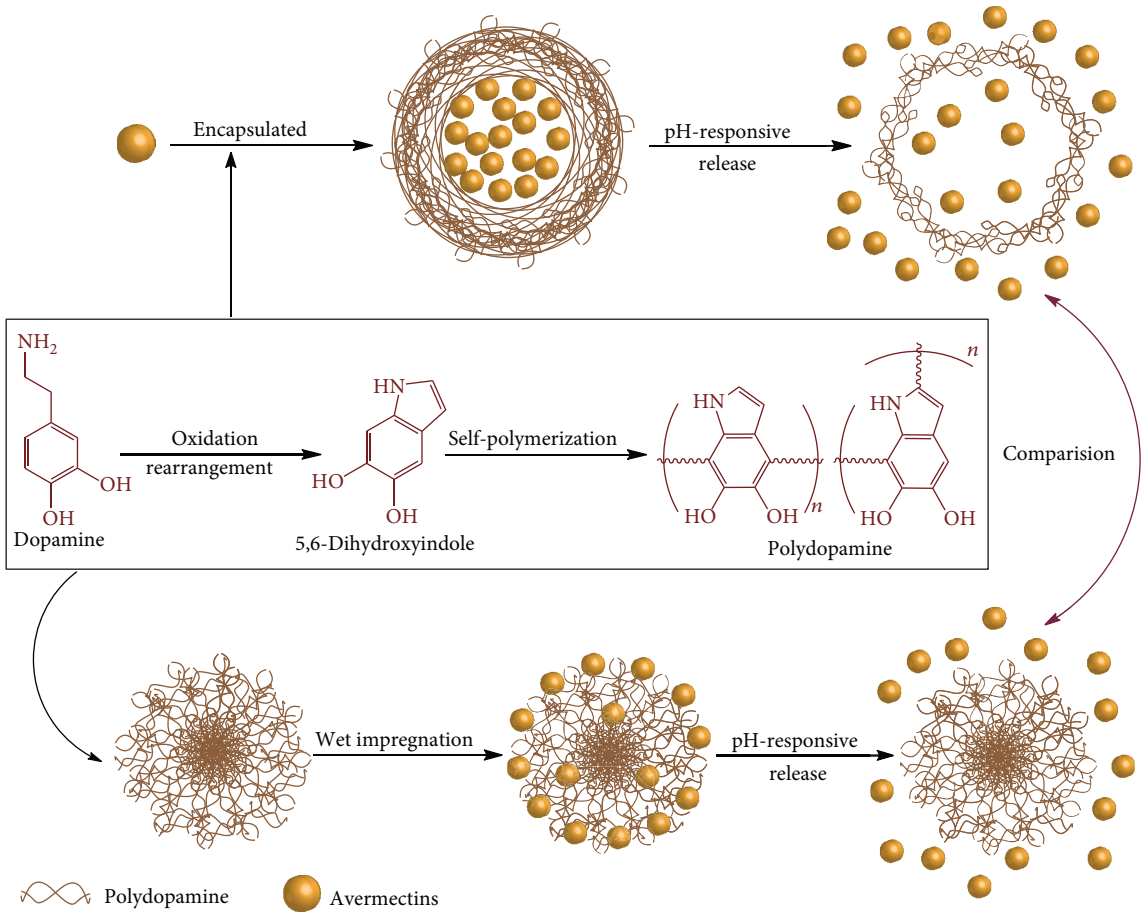

Scheme 1: Schematic illustration of the synthetic process of AVM@PDAMC and AVM/PDAMS.

150 mL of ethanol solution at 25°C under stirring for 3 min. Then, 1 mL of supernatant of the sample solution was transferred using a pipetting gun and an equal volume of the original ethanol solution was added to the flask to replace the withdrawn sample. After that, the reaction was stirred continuously for 24 h and 1 mL of supernatant of the sample solution was also transferred. The absorbance of the above two supernatants was obtained by a UV Lambda 365 ultraviolet-visible spectrometer, and the amount of AVM was calculated by the standard curvilinear equation above.

The following equation was used to calculate the LC of AVM@PDAMC:

$$\mathrm{LC} = \frac{[(C_{24} - C_3) \times V]}{M_2}, \tag{2}$$

where C_3 is the adsorption amount (mg/L) of AVM on the outer surface of PDAMC, C_{24} is the encapsulation amount (mg/L) of AVM encapsulated by PDAMC, V is the volume (L) of the ethanol solution, and M_2 is the mass (g) of PDAMC.

2.4. Antiultraviolet Properties of AVM/PDAMS and AVM@PDAMC. For m (mg), AVM/PDAMS or AVM@PDAMC was weighted and dispersed in a quartz Erlenmeyer flask with 50 mL of 40% ethanol solution at 25°C. A UV lamp (365 nm, 300 W) was used to degrade the above samples with a distance of 1 m. At intervals of t, 1 mL of the sample solution was transferred and diluted to 25 mL. An equal volume of the original solution was then added to the quartz Erlenmeyer flask to replace the withdrawn sample. The absorbance of the 25 mL solution was obtained. The absorbance was converted to the concentration with a standard curvilinear equation: $A = 0.0545C + 0.0468$; $R^2 = 0.9994$. Then, the residual amount of AVM was calculated as r_i. A $t - r_i$ curve was drawn to study the photodegradation of AVM. r_i was calculated as follows:

$$r_i = \begin{cases} 1 - \dfrac{[\rho_i \times 0.05]}{[m \times LC]} \ (i = 1), \\ 1 - \left\{ \dfrac{(\rho_i \times 0.05)}{(m \times LC)} + \dfrac{\left(\sum_{i=1}^{i-1} \rho_i \times 0.001\right)}{(m \times LC)} \right\} \ (i = 2, 3, 4 \ldots), \end{cases} \tag{3}$$

where ρ_i is the mass concentration (mg/L) of AVM for each sample.

2.5. Sustained Release Properties of AVM/PDAMS and AVM@PDAMC. For M (mg), AVM/PDAMS or AVM@PDAMC was weighted and dispersed in a conical flask with 50 mL of 40% ethanol solution at 25°C. At intervals of t, 1 mL of the sample solution was transferred and diluted to 25 mL. An equal volume of the original solution was then added to the conical flask to replace the withdrawn sample. A UV Lambda 365 ultraviolet-visible spectrometer was used to detect the absorbance of the 25 mL solution and the detected value was converted to the concentration with a standard curvilinear equation: $A = 0.0545C + 0.0468$; $R^2 = 0.9994$. Finally, the cumulative release amount of AVM was calculated as R_i and a sustained release curve was shown to study the release behavior of AVM/PDAMS and AVM@PDAMC. R_i was calculated as follows [32]:

$$R_i = \begin{cases} \dfrac{(\rho_i \times 0.05)}{(M \times LC)} \ (i = 1), \\ \dfrac{(\rho_i \times 0.05)}{(M \times LC)} + \dfrac{\sum_{i=1}^{i-1} \rho_i \times 0.001}{(M \times LC)} \ (i = 2, 3, 4 \ldots). \end{cases} \tag{4}$$

2.6. Statistical Analysis. A difference factor (f_1) and a similarity factor (f_2) were proposed to compare the differences and similarities between two in vitro dissolution profiles [33]. f_1 calculates the percent difference between the two curves at each time point, and it is a measurement of the relative error between the two curves. f_2 is a logarithmic reciprocal square root transformation of the sum of the squared error, and it is the measure of the similarity in the percent dissolution between the curves. When $f_1 > 15$ and $f_2 < 50$, there were significant differences between the two curves so that these two factors could be used for further analysis of the differences in sustained release of AVM@PDAMC and AVM/PDAMS. f_1 and f_2 were calculated as follows:

$$f_1 = 100 \left[\frac{\left(\sum_{i=1}^{n} \left| R_i - R_i' \right| \right)}{\sum_{i=1}^{n} R_i} \right], \tag{5}$$

$$f_2 = 50 \log \left\{ \left[1 + \left(\frac{1}{n} \right) \sum_{i=1}^{n} \left(R_i - R_i' \right)^2 \right]^{-0.5} \times 100 \right\}, \tag{6}$$

where n is the number of the time points, R_i is the dissolution value of the reference formulation at time I, and R_i' is the dissolution value of the test formulation at time i.

2.7. Characterization. The compositions of the particles were analyzed by a Spectrum 100 Fourier infrared spectrometer (PerkinElmer, Waltham, MA, USA) using the KBr squash technique. Before topographical characterization, samples were put in 10 mL ethanol with ultrasonic dispersion for 15 min to obtain a uniform suspension. Then, the upper suspension was dropped on the platform and dried. Gold particles were sprayed onto the surface of the samples under vacuum, and the samples were characterized by an S-4800 scanning electron microscope(Hitachi, Tokyo, Japan) to observe the surface topography. The zeta potential and particle size of the samples were investigated with a 90Plus PALS Zetasizer Nano ZS (Bruker Corporation, Karlsruhe, Germany) in water at pH = 7. Before investigating, samples were put in 5 mL ultrapure water with ultrasonic dispersion for 15 min to obtain a uniform suspension. A TGA 2 thermogravimetric analyzer (Mettler Toledo, Columbus, OH, USA) was used to analyze the heat stability of the particles over the heating range of 40–800°C and heating rate of 10°C·min^{-1}. A Q200 differential scanning calorimeter (TA Instruments, New Castle, DE, USA) was used to conduct differential scanning calorimetry (DSC) and detect the crystalline degree of avermectin in the particles over a heating range of 20–180°C and a heating rate of 10°C·min^{-1}.

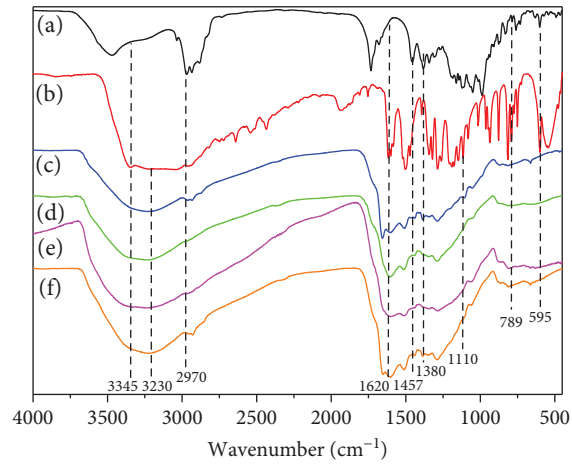

Figure 1: FTIR spectra of AVM (a), DA (b), AVM@PDAMC (c), AVM/PDAMS (d), PDAMS (e), and PDAMC (f).

Table 1: The particle diameters and zeta potential of PDAMS, PDAMC, AVM/PDAMS, AVM@PDAMC, and AVM.

Materials	Particle diameter (nm)	Polydispersity	Zeta potential (mV)
PDAMS	576.95	0.628	−40.05
PDAMC	583.40	0.540	−39.55
AVM/PDAMS	616.72	0.534	−50.41
AVM@PDAMC	643.64	0.556	−60.11
AVM	—	—	−28.12

3. Results and Discussion

3.1. Characterization. In Figure 1, Fourier transform infrared spectroscopy (FTIR) was adopted to compare the different compositions of DA, AVM, PDAMS, PDAMC, AVM/PDAMS, and AVM@PDAMC. For DA, the bands located at 3345 cm^{-1} and 3230 cm^{-1} were attributed to the stretching vibrations of phenolic amino and phenolic hydroxyl,

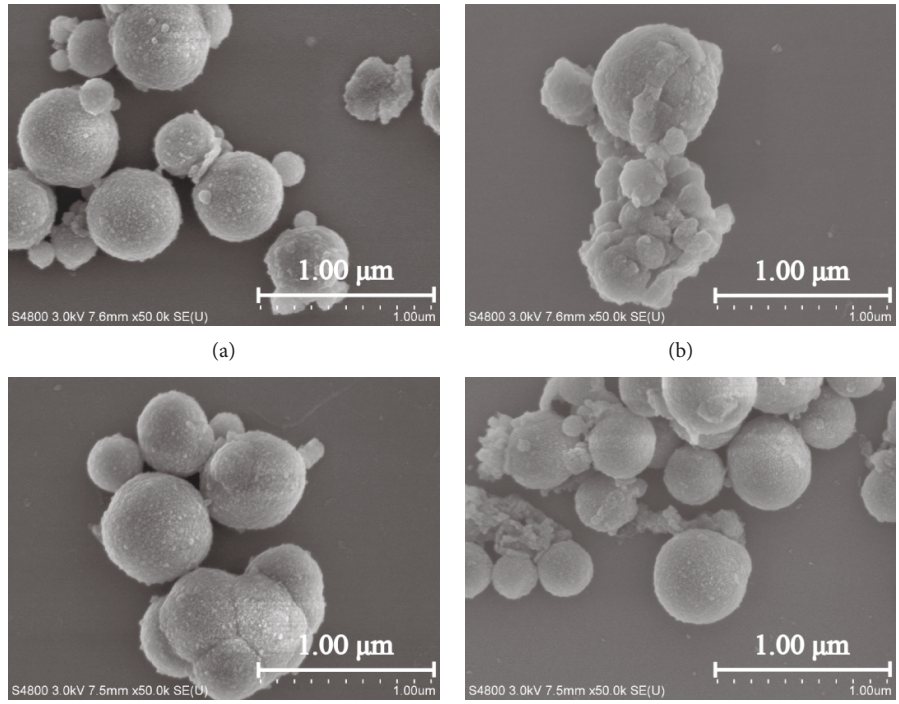

Figure 2: SEM images of PDAMS (a), PDAMC (b), AVM/PDAMS (c), and AVM@PDAMC (d).

respectively. The band that appeared at 1620 cm^{-1} was the stretching vibration of the benzene ring and the bending vibration of phenolic amino, respectively. The shear vibration band of the phenolic amino was located at 1520 cm^{-1}. The two bands that appeared at 1384 cm^{-1} and 1110 cm^{-1}belonged to the characteristic peaks of C-O-H and C-O on the phenolic hydroxyl. In comparison with DA, the characteristic peaks of indole and indoline structure were observed in the spectral line of PDAMS, PDAMC, AVM/PDAMS, and AVM@PDAMC, which confirmed the formation of polydopamine [34, 35]. Compared with AVM, the characteristic peaks located at 2970 cm^{-1}, 1457 cm^{-1}, 1380 cm^{-1}, 789 cm^{-1}, and 595 cm^{-1} belonged to C-H, and the heteroaromatic ring of AVM was observed in the spectral lines of AVM/PDAMS and AVM@PDAMC. This phenomenon meant that AVM had been successfully loaded on the PDAMS and PDAMC.

As listed in Table 1, the zeta potential of AVM/PDAMS shifted from −40.05 to −50.41 mV, while the zeta potential of AVM@PDAMC changed from −39.55 mV to −60.11 mV due to the loading of negatively charged AVM. Meanwhile, after loading AVM, the particle sizes of AVM/PDAMS and AVM@PDAMC increased to 39.77 nm and 56.64 nm, respectively. It was obvious that both the zeta potential and particle size of AVM@PDAMC had a greater change than that of AVM/PDAMS. This may be explained by the fact that AVM@PDAMC was loaded with more AVM. The polydispersity of all the samples were higher than 0.3, which was indicative of the wide distribution of nanoparticle size.

Figure 2 depicts the SEM images of PDAMS, PDAMC, AVM/PDAMS, and AVM@PDAMC. All the materials showed a spherical shape and the particle size distribution of the materials was generally between 480 and 560 nm. However, the particle sizes of a small part of the particles were in the range of about 200–300 nm, which may be related to the pH difference during the process of synthesis [12]. Such a phenomenon was inconsistent with the polydispersity in Table 1. In comparison with PDAMC in Figure 2(b), AVM@PDAMC in Figure 2(d) showed a better ballability performance. This phenomenon may be explained as follows: On one hand, AVM with a negative potential was dissolved in 1-butanol making these droplets generate electrostatic repulsion to each other so that they could be more stably dispersed, which was beneficial to the formation of spherical microcapsules. On the other hand, the π–π stacking between the AVM molecules and PDA molecules facilitated the coating of PDA on the surface of 1-butanol droplets. These two factors together made the AVM@PDAMC perform better ballability. Moreover, due to the adhesion of PDA, the phenomenon of adhesive agglomeration was observed among the particles [36]. In addition, the particle size from the SEM images did not corroborate well with DLS. This is because DLS is an intensity-based technique, whereas SEM is number-based, making them fundamentally different [37, 38]. DLS measures the R_H of the dispersed particles, whereas SEM provides the projected surface area based on how much of the incident electrons were reflected by the sample. Hence, the size obtained by SEM is usually smaller than that of DLS [39].

As shown in Figure 3, AVM/PDAMS and AVM@PDAMC were subjected to TGA to obtain thermal stability information. For PDAMS, PDAMC, AVM/PDAMS, and

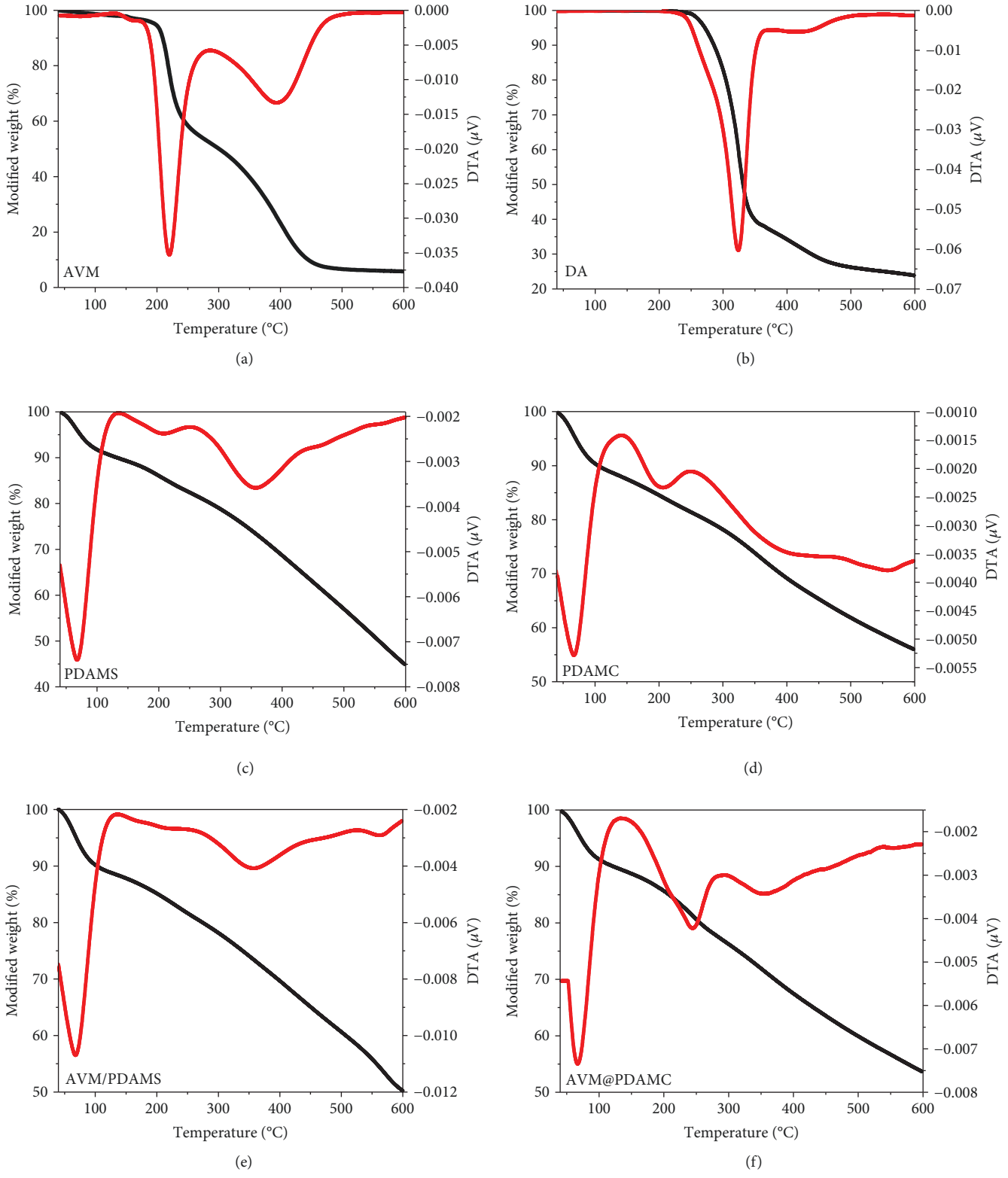

Figure 3: TG and DTG curves of AVM (a), DA (b), PDAMS (c), PDAMC (d), AVM/PDAMS (e), and AVM@PDAMC (f).

AVM@PDAMC, the loss in mass from 50°C to 100°C was due to the elimination of residual physically adsorbed water. No sharp peak of thermal decomposition was observed during the subsequent heating process, which indicated that DA molecules were polymerized into PDA through the formation of covalent bonds [40]. Compared to the curves of

AVM, PDAMS, and PDAMC, the loss in mass from 200 to 600°C of AVM/PDAMS and AVM@PDAMC was caused by the deposition of AVM and PDA. The thermal decomposition peak of AVM loaded on PDAMS and PDAMC was not obvious and both of them shifted from 220°C to 235°C and 245°C, respectively, which indicated the improvement in the thermal stability of AVM. Moreover, the thermal decomposition temperature of AVM loaded on PDAMC was higher than that of PDAMS. This means that, in comparison to the direct adsorption effect of PDAMS, the coating effect of PDAMC could better improve the thermal stability of AVM as it avoids direct contact between AVM and the external environment.

Figure 4 exhibits the DSC thermograms of AVM and polydopamine materials. After the load of AVM, the melting peak of AVM/PDAMS increased from 105°C to 108°C, while the melting temperature of AVM@PDAMC shifted from 110°C to 116°C. The increase of the melting temperatures of these two kinds of materials may be due to the higher melting point of AVM (150–155°C, CAS, 71751-41-2) and the π–π stacking effect between AVM and PDA. It also confirmed that AVM was successfully loaded on PDA. The melting temperature change of AVM@PDAMC was greater than that of AVM/PDAMS, indicating that the coating method makes the interaction between AVM and PDA more effective than that of the adsorption method.

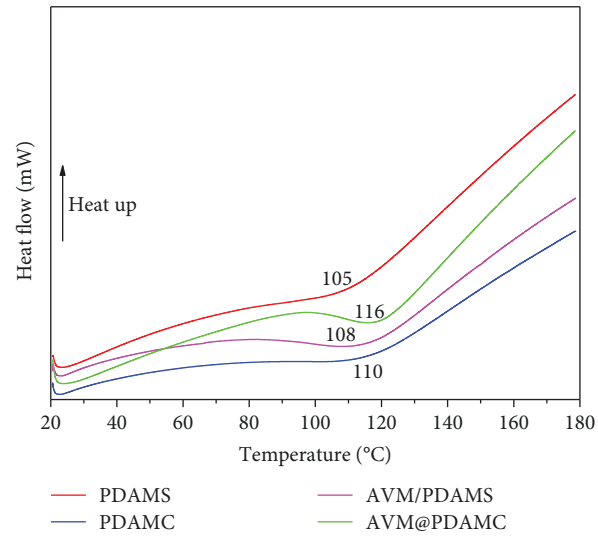

Figure 4: DSC curves of PDAMS, PDAMC, AVM/PDAMS, and AVM@PDAMC.

3.2. Study of Antiultraviolet Properties. Figure 5 shows the drug release residual curves of AVM, AVM/PDAMS, and AVM@PDAMC under ultraviolet radiation. After being irradiated with UV light for 200 min for both AVM/PDAMS and AVM@PDAMC, the residual AVM in solution began to reach equilibrium. Moreover, the residual AVM of AVM/PDAMS was less than 50% since 600 min, while that of AVM@PDAMC remained above 50% until 1400 min and the pure AVM had been degraded by 89% at the same time. This comparison on residual AVM between AVM/PDAMS and AVM@PDAMC indicated that the PDA vehicle could improve the UV resistance of AVM, and PDAMC provided significantly better UV resistance than PDAMS. It further demonstrated that when compared to the directed adsorption effect of the outer surface of PDAMS, the coating method could make PDA exert a shielding effect against ultraviolet irradiation and minimize the degradation effect of UV light to AVM.

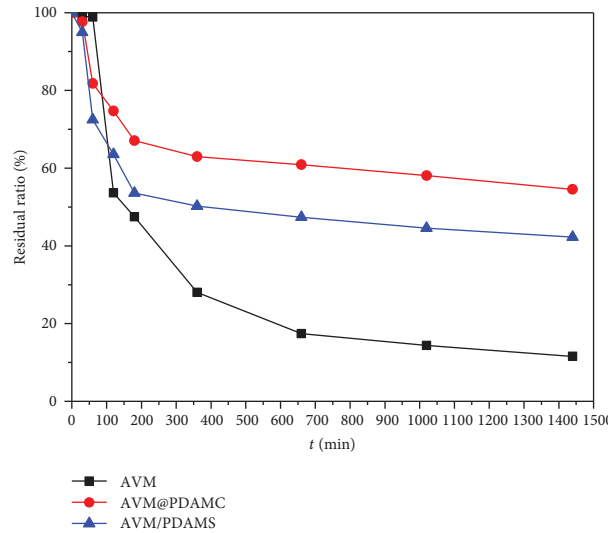

Figure 5: The residual ratio of AVM/PDAMS and AVM@PDAMC under irradiation of UV light.

3.3. Sustained Release Performance Study. The AVM release profiles of AVM/PDAMS and AVM@PDAMC at different pH values are shown in Figure 6. It was clear that both AVM/PDAMS and AVM@PDAMC showed significant pH responsiveness. They all performed the fastest release at pH 3 and the slowest release at pH 7. Moreover, at pH 3, the release of AVM from AVM/PDAMS reached the 50% cumulative release rate (R_i) at 13 h, while that of AVM@PDAMC needed an additional 47 h. At pH 9, AVM released from AVM/PDAMS needed 50 h to reach 50% of R_i, while it took 90 h to make that of AVM@PDAMC reach the same rate. AVM/PDAMS spent 59 h reaching 50% of R_i at pH 7, while AVM@PDAMC did not reach the same R_i until 150 h. In general, AVM@PDAMC achieved a better sustained release effect than AVM/PDAMS.

Theoretically speaking [36], PDA usually carries a positive charge due to the protonation of amino groups under acidic conditions so that the AVM molecule with a negative charge can combine closely with the PDA vehicle. This factor would make the release of AVM from the PDA vehicles perform slower at pH 3 than that at pH 9. However, our experimental result was different. So, the possible sustained release mechanism of our PDA systems could be explained as follows: at pH 7, the AVM with a large amount of heteroaromatic rings and hydroxyl groups could form π–π stacking structures and hydrogen bonds with the phenol structure and amino group of PDA, so that the AVM could be

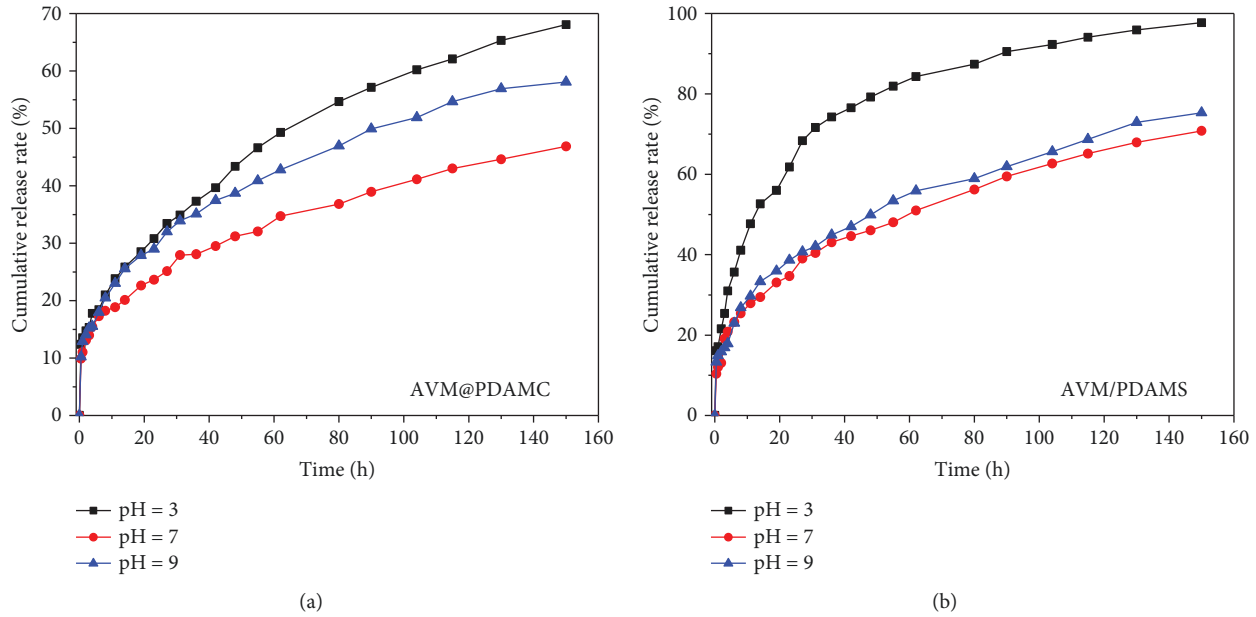

Figure 6: Release curves of AVM/PDAMS (a) and AVM@PDAMC (b) under different pH values.

Table 2: Statistical variability results for the release kinetic of AVM/PDAMS and AVM@PDAMC under the same pH.

Fit factors	pH = 3	pH = 7	pH = 9
f_1	42.35	30.60	20.21
f_2	26.89	43.99	51.00

Table 3: Release kinetic models of drug release.

Release model	Formulation
Zero-order model	$y = K_1 t$
First-order model	$y = K_2[1 - \exp(-K_1 t)]$
Hixson–Crowell model	$y = (K_2 - K_1 t)^3$
Weibull model	$y = 1 - \exp\left[\left(-t^{K_2}\right)/K_1\right]$
Higuchi model	$y = K_1 t^{1/2}$
Baker–Lonsdale model	$(3/2)\left[1 - (1-y)^{2/3}\right] - y = K_1 t$
Korsmeyer–Peppas model	$y = K_2 t^{K_1}$
Quadratic model	$y = 100\left(K_1 t^2 + K_2 t\right)$
Logistic model	$y = K_3/\{1 + \exp[-K_2(t - K_1)]\}$

adsorbed or encapsulated effectively by PDA [41, 42]. On the contrary, when the release environment was acidic, the π–π stacking and the hydrogen bond were destroyed, and the PDA molecules underwent protonation, which reduced the interaction among the PDA chains, resulting in the stretch of the molecular chain structure and the enlargement of the molecular distance, finally leading to the loose union between AVM and PDA. The influence of this destructive effect exceeded the electrostatic attraction between the protonated PDA and the AVM, which caused a macroscopic phenomenon of accelerating the release of AVM. Under basic conditions, on one hand, the deprotonated PDA with a negative charge showed an electrostatic repulsion to AVM; on the other hand, mutual interaction generated by the π–π stacking and hydrogen bond limited the diffusion of AVM from the PDA vehicle into the solution. These two forces competed with each other, eventually leading to a sustained release rate that was faster than that of the neutral condition, but slower than that of the basic environment. In addition, when compared to the directed adsorption of PDAMS for AVM, PDAMC encapsulated the AVM in its hollow cavity, which meant that the release of AVM was not only controlled by the charge properties and the π–π stacking of PDA, but was also restricted by the barrier effect of the PDA coating [43]. Therefore, the controlled release performance of PDAMC for AVM was better than that of PDAMS.

The above results proved that the systems performed the higher release rate at lower pH and the lower release of pesticide at neutral pH. This fact indicated that the AVM/PDAMS system can be well stored in a neutral environment and activated while sprayed into earth under acidic conditions such as the red clay in Southern China [44], while AVM@PDAMC can also be activated in soil under basic environmental conditions.

3.4. Statistical Analysis. The results of f_1 and f_2 are listed in Table 2. It was clear that at pH 3 and pH 7, the sustained release of AVM/PDAMS and AVM@PDAMC was obviously different, while at pH 9 this was not obvious. This showed that different release environments had different degrees of influence on these two kinds of materials.

3.5. Study of Release Kinetics. In order to further study the release regulars of AVM/PDAMS and AVM@PDAMC,

Table 4: Fitting results for release curves of AVM/PDAMS and AVM@PDAMC.

Release model	pH	AVM@PDAMC				AVM/PDAMS			
		K_1	K_2	K_3	R^2	K_1	K_2	K_3	R^2
Zero-order model	3	0.0042	—	—	0.9635	0.0053	—	—	0.7433
	7	0.0024	—	—	0.9148	0.0035	—	—	0.8898
	9	0.0031	—	—	0.8918	0.0040	—	—	0.8734
First-order model	3	0.0227	0.6857	—	0.8667	0.0639	0.8870	—	0.9279
	7	0.0485	0.3953	—	0.7429	0.0498	0.5726	—	0.7971
	9	0.0455	0.4932	—	0.8321	0.0438	0.6307	—	0.8765
Hixson–Crowell model	3	0.0023	0.5963	—	0.9027	0.0020	0.7593	—	0.6685
	7	0.0016	0.5662	—	0.8586	0.0018	0.6413	—	0.8275
	9	0.0018	0.5994	—	0.8297	0.0020	0.6430	—	0.8064
Weibull model	3	15.7661	0.5727	—	0.9538	6.2909	0.5922	—	0.9951
	7	10.8111	0.3710	—	0.9825	7.8666	0.4169	—	0.9861
	9	10.0934	0.4199	—	0.9886	9.1389	0.4799	—	0.9930
Higuchi model	3	0.0606	—	—	0.9666	0.1005	—	—	0.7808
	7	0.0432	—	—	0.8259	0.0627	—	—	0.8367
	9	0.0530	—	—	0.8813	0.0671	—	—	0.9119
Baker–Lonsdale model	3	8.7246×10^{-4}	—	—	0.9935	0.0030	—	—	0.9811
	7	3.4348×10^{-4}	—	—	0.9840	8.2042×10^{-4}	—	—	0.9866
	9	5.5707×10^{-4}	—	—	0.9871	0.0010	—	—	0.9919
Korsmeyer–Peppas model	3	0.4392	0.0785	—	0.9750	0.3072	0.2269	—	0.9717
	7	0.3154	0.0941	—	0.9898	0.3184	0.1350	—	0.9950
	9	0.3380	0.1051	—	0.9938	0.3539	0.1247	—	0.9967
Quadratic model	3	-4.5900×10^{-7}	1.1162×10^{-4}	—	0.8162	-1.1684×10^{-6}	2.2483×10^{-4}	—	0.5998
	7	-4.1335×10^{-7}	8.7622×10^{-5}	—	0.4807	-6.2282×10^{-7}	1.2960×10^{-4}	—	0.5316
	9	-5.0533×10^{-7}	1.0750×10^{-4}	—	0.6004	-6.4022×10^{-7}	1.3630×10^{-4}	—	0.6741
Logistic model	3	38.0052	0.0329	0.7066	0.9934	13.4592	0.0772	0.9055	0.9679
	7	22.0411	0.0354	0.4440	0.9693	19.5788	0.0419	0.6222	0.9699
	9	20.9608	0.0430	0.5287	0.9594	21.3379	0.0467	0.6653	0.9502

several kinetic models (Table 3) were applied to fit the release data [45, 46]. The results are shown in Table 4 and Figures 7 and 8. From R^2, at pH 7 and pH 9, the release processes of both AVM/PDAMS and AVM@PDAMC were more in accordance with the Korsmeyer–Peppas equation, and their value of K_1 was smaller than 0.45, indicating that the release behaviors were controlled by the Fick diffusion. Moreover, their release processes tended to be a one-way release. The result also showed that there was an exponentially decreasing concentration gradient from the center of the vehicle to the surrounding environment during the release of AVM, and the PDA chains were tightly bound to each other [47]. In contrast, at pH 3, the release behavior of AVM@PDAMC fitted the Baker–Lonsdale model and illustrated that AVM@PDAMC maintained its original good spherical appearance without collapse as the model was suitable for the release process of spherical nanodrug delivery systems [47]. AVM/PDAMS was in line with the Weibull model, and $K_2 < 1$, which indicated that the fitting curve had a higher initial slope, reflecting the large release of AVM adsorbed on the surface of PDAMS during the sustained release.

4. Conclusion

In this paper, AVM/PDAMS and AVM@PDAMC were designed and prepared to investigate antiultraviolet performance and sustained release behaviors. The materials all had a spherical appearance. The application of PDA facilitated the improvement of the thermal stability of AVM. The coating effect of PDAMC not only made the thermal stability of AVM more enhanced, but it also improved the loading amount of PDA for AVM. AVM@PDAMC exhibited better UV resistance than AVM/PDAMS, and the formation of the PDA coating improved the UV-shielding effect of the system. At pH 7 and pH 9, the sustained release process of AVM@PDAC and AVM/PDAMS could be described by the Korsmeyer–Peppas equation and followed the Fick diffusion. At pH 3, the Baker–Lonsdale model and the Weibull model could be applied to explain the release behaviors of AVM@PDAMC and AVM/PDAMS, respectively. Under acidic conditions, the release rate of both AVM@pDAMC and AVM/PDAMS increased. The time required for AVM/PDAMS to reach 50% of R_i was 47 h earlier than that of AVM@PDAMC, while at pH 7, the R_i of

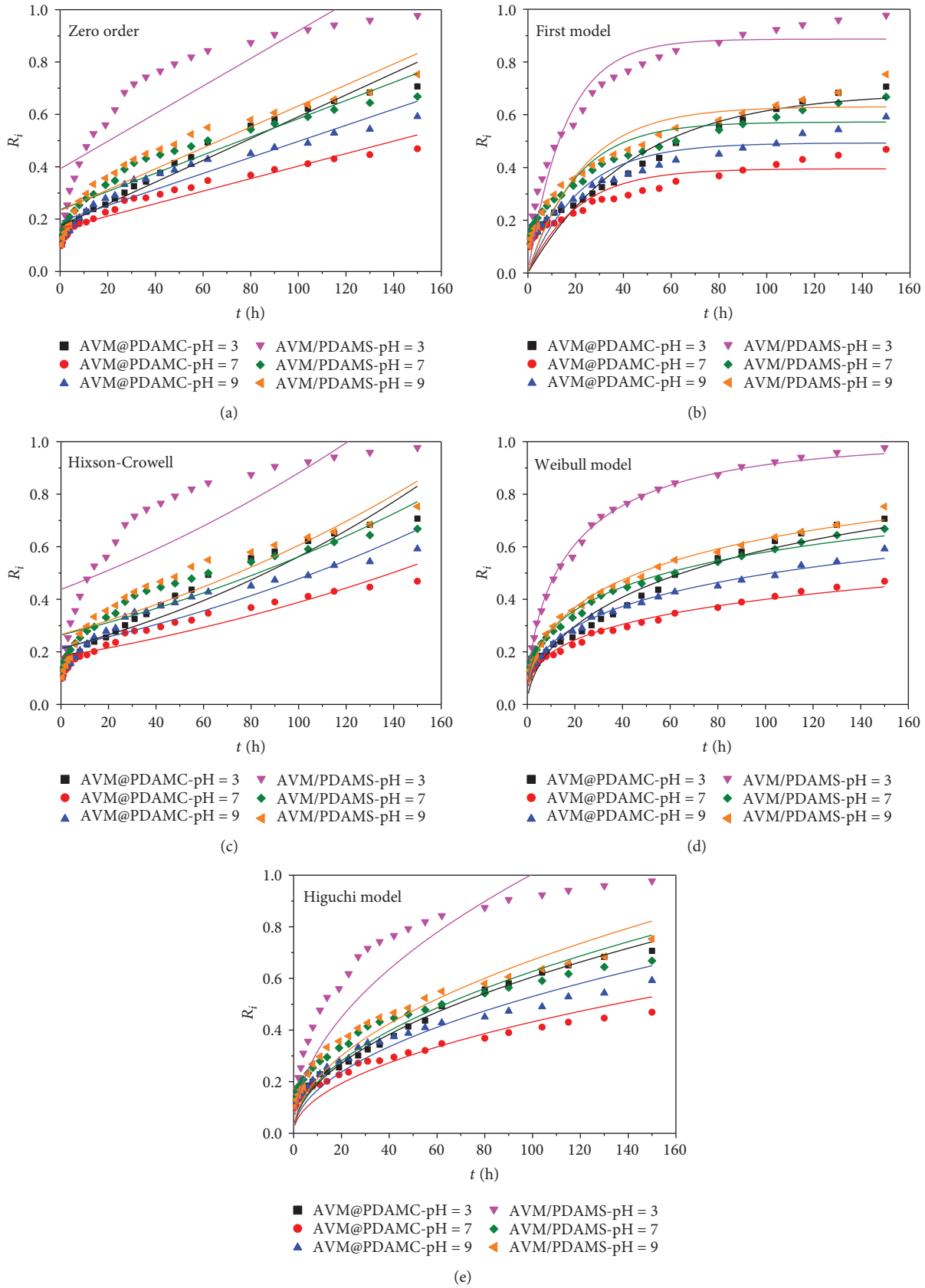

Figure 7: Nonlinear fit of release curves of AVM/PDAMS and AVM@PDAMC.

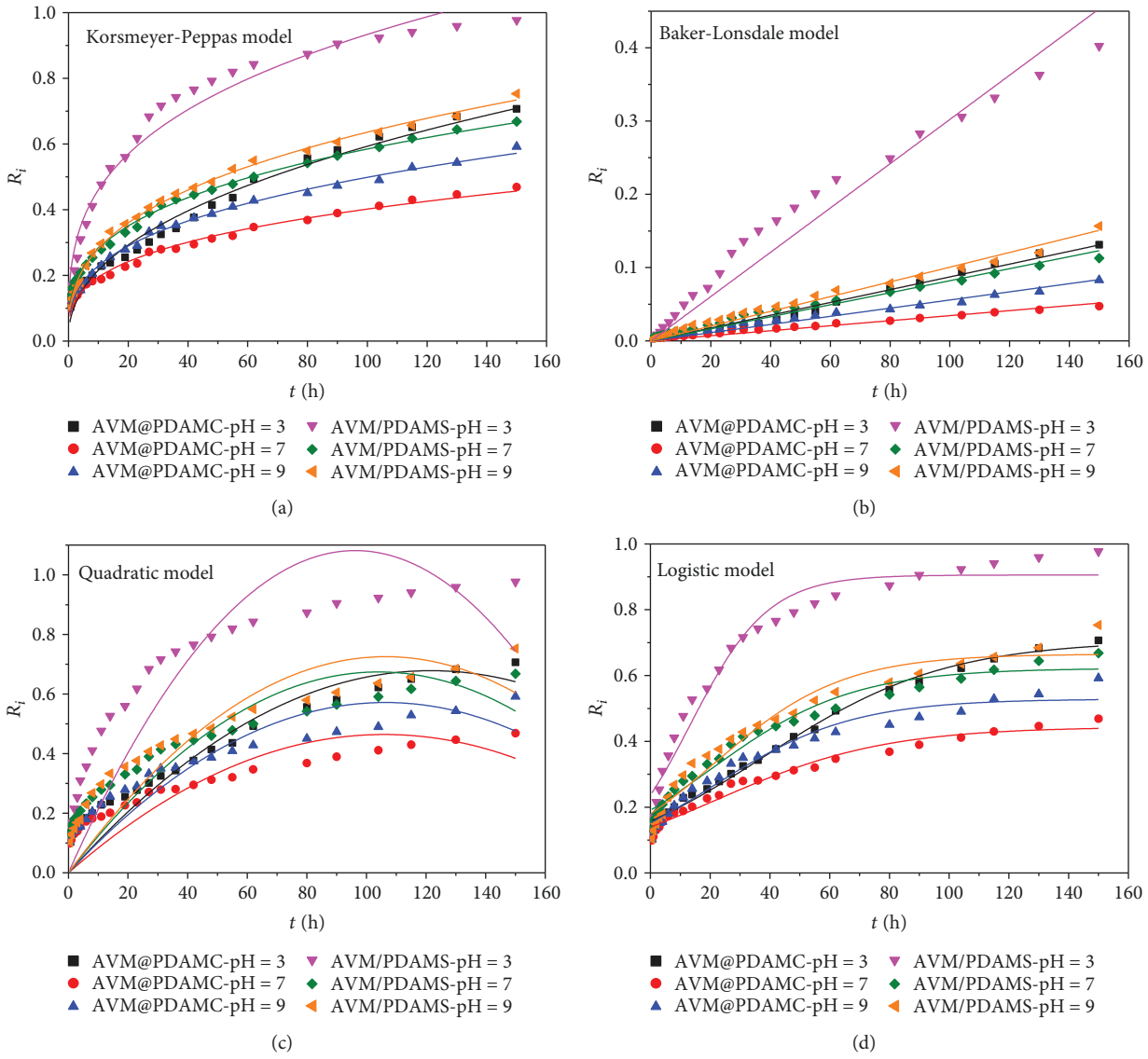

Figure 8: Nonlinear fit of release curves of AVM/PDAMS and AVM@PDAMC.

AVM@PDAMC did not reach 50% during the whole process. PDAMC exhibited superior controllability for AVM over PDAMS. The π–π stacking played a key role in the controlled release of AVM from the PDA vehicle and created a competitive relationship with the electrostatic interactions between AVM and PDA. This polydopamine drug delivery system with a controlled release of pesticides has potential application value in the agricultural field with the stimulation caused by the changes of the soil environment or the physiological system of pests.

Data Availability

The excel data used to support the findings of this study have been deposited in the Scientific Data's List of Recommended Repositories. Here is the link: https://figshare.com/s/c3b49caebe963dc93975.

Conflicts of Interest

The authors declare no competing financial interest.

Authors' Contributions

Zhichuan Shen and Xinhua Zhou conceived and designed the experiments. Huina Qiu performed the experiments. Zhichuan Shen, Hongjun Zhou, and Xinhua Zhou analyzed the data. Hua Xu and Huayao Chen provided the reagents/-materials. Zhichuan Shen, Hongjun Zhou, and Xinhua Zhou wrote/edited the paper.

Acknowledgments

This research was funded by the National Natural Science Foundation of China (Grant no. 21576303), the Natural Science Foundation of Guangdong Province (Grant no.

2016A030313375, 2017A030311003), the Science and Technology Program of the Department of Agriculture of Guangdong Province (Grant no. 2017LM4177), and the Climbing Program for Students in the Universities of Guangdong Province (Grant no. pdjh2017b0255).

Supplementary Materials

Graphic abstract. The polydopamine microcapsule had a better release control property for avermectin than the polydopamine microsphere. At pH 3, the polydopamine microcapsule and polydopamine microsphere showed sensitive release for avermectin and followed the Baker–Lonsdale model and the Weibull model, respectively. The polydopamine microcapsule had a better anti-UV capability for avermectin than the polydopamine microsphere. *(Supplementary Materials)*

References

[1] M. G. Mogul, H. Akin, N. Hasirci, D. J. Trantolo, J. D. Gresser, and D. L. Wise, "Controlled release of biologically active agents for purposes of agricultural crop management," *Resources, Conservation and Recycling*, vol. 16, no. 1-4, pp. 289–320, 1996.

[2] J. Gan, M. Hussain, and N. M. Rathor, "Behaviour of an alginate-kaolin based controlled-release formulation of the herbicide thiobencarb in simulated ecosystems," *Pesticide Science*, vol. 42, no. 4, pp. 265–272, 1994.

[3] M. Margni, D. Rossier, P. Crettaz, and O. Jolliet, "Life cycle impact assessment of pesticides on human health and ecosystems," *Agriculture, Ecosystems and Environment*, vol. 93, no. 1-3, pp. 379–392, 2002.

[4] Z.-Z. Li, S. A. Xu, L. X. Wen et al., "Controlled release of avermectin from porous hollow silica nanoparticles: influence of shell thickness on loading efficiency, UV-shielding property and release," *Journal of Controlled Release*, vol. 111, no. 1-2, pp. 81–88, 2006.

[5] S. He, W. Zhang, D. Li et al., "Preparation and characterization of double-shelled avermectin microcapsules based on copolymer matrix of silica–glutaraldehyde–chitosan," *Journal of Materials Chemistry B*, vol. 1, no. 9, pp. 1270–1278, 2013.

[6] R. Issa, A. Akelah, A. Rehab, R. Solaro, and E. Chiellini, "Controlled release of herbicides bound to poly(oligo(oxyethylene) methacrylate) hydrogels," *Journal of Controlled Release*, vol. 13, no. 1, pp. 1–10, 1990.

[7] N. A. Peppas and R. Langer, "New challenges in biomaterials," *Science*, vol. 263, no. 5154, pp. 1715–1720, 1994.

[8] S. Hong, Y. S. Na, S. Choi, I. T. Song, W. Y. Kim, and H. Lee, "Non-covalent self-assembly and covalent polymerization co-contribute to polydopamine formation," *Advanced Functional Materials*, vol. 22, no. 22, pp. 4711–4717, 2012.

[9] J. K. Beattie, A. M. Djerdjev, A. Gray-Weale et al., "PH and the surface tension of water," *Journal of Colloid and Interface Science*, vol. 422, pp. 54–57, 2014.

[10] J. Cui, Y. Yan, G. K. Such et al., "Immobilization and intracellular delivery of an anticancer drug using mussel-inspired polydopamine capsules," *Biomacromolecules*, vol. 13, no. 8, pp. 2225–2228, 2012.

[11] B. Yu, D. A. Wang, Q. Ye, F. Zhou, and W. Liu, "Robust polydopamine nano/microcapsules and their loading and release behavior," *Chemical Communications*, no. 44, pp. 6789–6791, 2009.

[12] C.-C. Ho and S.-J. Ding, "The pH-controlled nanoparticles size of polydopamine for anti-cancer drug delivery," *Journal of Materials Science: Materials in Medicine*, vol. 24, no. 10, pp. 2381–2390, 2013.

[13] T. Tamanna and A. Yu, "Polydopamine nanoparticle as a stable and capacious nano-reservoir of rifampicin," *International Journal of Medical, Health, Biomedical, Bioengineering and Pharmaceutical Engineering*, vol. 10, no. 2, pp. 35–38, 2016.

[14] Q. Liu, B. Yu, W. Ye, and F. Zhou, "Highly selective uptake and release of charged molecules by pH-responsive polydopamine microcapsules," *Macromolecular Bioscience*, vol. 11, no. 9, pp. 1227–1234, 2011.

[15] K. Kono, K. Kawakami, K. Morimoto, and T. Takagishi, "Effect of hydrophobic units on the pH-responsive release property of polyelectrolyte complex capsules," *Journal of Applied Polymer Science*, vol. 72, no. 13, pp. 1763–1773, 1999.

[16] A. Lamprecht, H. Yamamoto, H. Takeuchi, and Y. Kawashima, "Microsphere design for the colonic delivery of 5-fluorouracil," *Journal of Controlled Release*, vol. 90, no. 3, pp. 313–322, 2003.

[17] A. Stefanache, M. Ignat, C. Peptu, A. Diaconu, I. Stoleriu, and L. Ochiuz, "Development of a prolonged-release drug delivery system with magnolol loaded in amino-functionalized mesoporous silica," *Applied Sciences*, vol. 7, no. 3, p. 237, 2017.

[18] M. d'Ischia, A. Napolitano, V. Ball, C. T. Chen, and M. J. Buehler, "Polydopamine and eumelanin: from structure–property relationships to a unified tailoring strategy," *Accounts of Chemical Research*, vol. 47, no. 12, pp. 3541–3550, 2014.

[19] Y. Liu, K. Ai, and L. Lu, "Polydopamine and its derivative materials: synthesis and promising applications in energy, environmental, and biomedical fields," *Chemical Reviews*, vol. 114, no. 9, pp. 5057–5115, 2014.

[20] K.-Y. Ju, Y. Lee, S. Lee, S. B. Park, and J. K. Lee, "Bioinspired polymerization of dopamine to generate melanin-like nanoparticles having an excellent free-radical-scavenging property," *Biomacromolecules*, vol. 12, no. 3, pp. 625–632, 2011.

[21] K. Shanmuganathan, J. H. Cho, P. Iyer, S. Baranowitz, and C. J. Ellison, "Thermooxidative stabilization of polymers using natural and synthetic melanins," *Macromolecules*, vol. 44, no. 24, pp. 9499–9507, 2011.

[22] J.-J. Feng, P. P. Zhang, A. J. Wang, Q. C. Liao, J. L. Xi, and J. R. Chen, "One-step synthesis of monodisperse polydopamine-coated silver core–shell nanostructures for enhanced photocatalysis," *New Journal of Chemistry*, vol. 36, no. 1, pp. 148–154, 2012.

[23] S. L. Phua, L. Yang, C. L. Toh et al., "Simultaneous enhancements of UV resistance and mechanical properties of polypropylene by incorporation of dopamine-modified clay," *ACS Applied Materials & Interfaces*, vol. 5, no. 4, pp. 1302–1309, 2013.

[24] S. Xiong, Y. Wang, J. Yu, L. Chen, J. Zhu, and Z. Hu, "Polydopamine particles for next-generation multifunctional biocomposites," *Journal of Materials Chemistry A*, vol. 2, no. 20, pp. 7578–7587, 2014.

[25] R. W. Burg, B. M. Miller, E. E. Baker et al., "Avermectins, new family of potent anthelmintic agents: producing organism and fermentation," *Antimicrobial Agents and Chemotherapy*, vol. 15, no. 3, pp. 361–367, 1979.

[26] L. S. Crouch, W. F. Feely, B. H. Arison et al., "Photodegradation of Avermectin B1a thin films on glass," *Journal of Agricultural and Food Chemistry*, vol. 39, no. 7, pp. 1310–1319, 1991.

[27] Y. Li, M. Zhou, Y. Pang, and X. Qiu, "Lignin-based microsphere: preparation and performance on encapsulating the pesticide avermectin," *ACS Sustainable Chemistry & Engineering*, vol. 5, no. 4, pp. 3321–3328, 2017.

[28] Q. Yue, M. Wang, Z. Sun et al., "A versatile ethanol-mediated polymerization of dopamine for efficient surface modification and the construction of functional core–shell nanostructures," *Journal of Materials Chemistry B*, vol. 1, no. 44, pp. 6085–6093, 2013.

[29] J. Yan, L. Yang, M. F. Lin, J. Ma, X. Lu, and P. S. Lee, "Polydopamine spheres as active templates for convenient synthesis of various nanostructures," *Small*, vol. 9, no. 4, pp. 596–603, 2013.

[30] H. Chen, Y. Lin, H. Zhou, X. Zhou, S. Gong, and H. Xu, "Synthesis and characterization of chlorpyrifos/copper(II) Schiff base mesoporous silica with pH sensitivity for pesticide sustained release," *Journal of Agricultural and Food Chemistry*, vol. 64, no. 43, pp. 8095–8102, 2016.

[31] C. Huayao, L. Yueshun, Z. Hongjun, Z. Xinhua, G. Sheng, and X. Hua, "Highly efficient alginate sodium encapsulated chlorpyrifos/copper(II) Schiff base mesoporous silica sustained release system with pH and ion response for pesticide delivery," *RSC Advances*, vol. 6, no. 115, pp. 114714–114721, 2016.

[32] H. Chen, Y. Lin, H. Xu et al., "Preparation of sustained-release chlorpyrifos particles via the emulsification coacervation method and their sustained-release performance," *Journal of Macromolecular Science, Part A*, vol. 54, no. 2, pp. 91–96, 2017.

[33] V. Pillay and R. Fassihi, "Evaluation and comparison of dissolution data derived from different modified release dosage forms: an alternative method," *Journal of Controlled Release*, vol. 55, no. 1, pp. 45–55, 1998.

[34] X. Zheng, J. Zhang, J. Wang, X. Qi, J. M. Rosenholm, and K. Cai, "Polydopamine coatings in confined nanopore space: toward improved retention and release of hydrophilic cargo," *Journal of Physical Chemistry C*, vol. 119, no. 43, pp. 24512–24521, 2015.

[35] N. Nishizawa, A. Kawamura, M. Kohri, Y. Nakamura, and S. Fujii, "Polydopamine particle as a particulate emulsifier," *Polymer*, vol. 8, no. 3, p. 62, 2016.

[36] X. Jia, W. Sheng, W. Li, Y. Tong, Z. Liu, and F. Zhou, "Adhesive polydopamine coated avermectin microcapsules for prolonging foliar pesticide retention," *ACS Applied Materials & Interfaces*, vol. 6, no. 22, pp. 19552–19558, 2014.

[37] X. Zhao, S. Zhu, Y. Song, J. Zhang, and B. Yang, "Thermal responsive fluorescent nanocomposites based on carbon dots," *RSC Advances*, vol. 5, no. 20, pp. 15187–15193, 2015.

[38] K.-H. Kim, H. Xing, J. M. Zuo, P. Zhang, and H. Wang, "TEM based high resolution and low-dose scanning electron nanodiffraction technique for nanostructure imaging and analysis," *Micron*, vol. 71, pp. 39–45, 2015.

[39] S. Bhattacharjee, "DLS and zeta potential—what they are and what they are not?," *Journal of Controlled Release*, vol. 235, pp. 337–351, 2016.

[40] R. Batul, T. Tamanna, A. Khaliq, and A. Yu, "Recent progress in the biomedical applications of polydopamine nanostructures," *Biomaterials Science*, vol. 5, no. 7, pp. 1204–1229, 2017.

[41] J. Fu, Z. Chen, M. Wang et al., "Adsorption of methylene blue by a high-efficiency adsorbent (polydopamine microspheres): kinetics, isotherm, thermodynamics and mechanism analysis," *Chemical Engineering Journal*, vol. 259, pp. 53–61, 2015.

[42] H. Gao, Y. Sun, J. Zhou, R. Xu, and H. Duan, "Mussel-inspired synthesis of polydopamine-functionalized graphene hydrogel as reusable adsorbents for water purification," *ACS Applied Materials & Interfaces*, vol. 5, no. 2, pp. 425–432, 2013.

[43] W. Sheng, W. Li, G. Zhang, Y. Tong, Z. Liu, and X. Jia, "Study on the UV-shielding and controlled-release properties of a polydopamine coating for avermectin," *New Journal of Chemistry*, vol. 39, no. 4, pp. 2752–2757, 2015.

[44] H. Liu, X. Wu, Q. Wang, S. Wang, D. Liu, and G. Liu, "Responses of soil ammonia oxidation and ammonia-oxidizing communities to land-use conversion and fertilization in an acidic red soil of southern China," *European Journal of Soil Biology*, vol. 80, pp. 110–120, 2017.

[45] F. O. Costa, J. J. S. Sousa, A. A. C. C. Pais, and S. J. Formosinho, "Comparison of dissolution profiles of ibuprofen pellets," *Journal of Controlled Release*, vol. 89, no. 2, pp. 199–212, 2003.

[46] P. Costa and J. M. Sousa Lobo, "Modeling and comparison of dissolution profiles," *European Journal of Pharmaceutical Sciences*, vol. 13, no. 2, pp. 123–133, 2001.

[47] M. L. Bruschi, *Mathematical Models of Drug Release*, Elsevier Science, Amsterdam, 2015.